This is a preprint, the final version is subject to change, of the American Mineralogist (MSA)
Cite as Authors (Year) Title. American Mineralogist, in press.
(DOI will not work until issue is live.) DOI: http://dx.doi.org/10.2138/am-2016-5575

Revision 1

Esperance: Multiple Episodes of Aqueous Alteration Involving Fracture Fills and Coatings at Matijevic Hill, Mars.

Corresponding Author: Benton C. Clark, Space Science Institute, 4750 Walnut, Boulder, CO 80301, USA (bclark@ spacescience.org)

RichardV. Morris, NASA/Johnson Space Center, Houston, TX 77058, USA; richard.v.morris@nasa.gov

Kenneth E. Herkenhoff, USGS Astrogeology Science Center, Flagstaff, AZ 86001, USA; kherkenhoff@usgs.gov

William H. Farrand, Space Science Institute, Boulder, CO 80301, USA; farrand@SpaceScience.org

Ralf Gellert, Univ. of Guelph, Guelph, ON, N1G2W1, Canada; ralf@physics.uoguelph.ca

Bradley L. Jolliff, Washington University in St. Louis, St. Louis, MO, 63130, USA; bradjolliff@gmail.com

Raymond E. Arvidson, Washington University in St. Louis, St. Louis, MO, 63130, USA; arvidson@wunder.wustl.edu

Steven W. Squyres, Cornell University, Ithaca, NY, 14853, USA; squyres@astro.cornell.edu

David W. Mittelfehldt, NASA/Johnson Space Center, Houston, TX 77058, USA; david.w.mittlefehldt@nasa.gov

Douglas W. Ming, NASA/Johnson Space Center, Houston, TX 77058, USA; douglas.w.ming@nasa.gov

Albert S. Yen, Jet Propulsion Laboratory, Pasadena, CA 91109, USA; albert.s.yen@jpl.nasa.gov

Key Points:

Veins and coatings indicate multiple aqueous episodes on Mars

Multiple habitats for life on Mars

These previous inhabitable locations not observable from orbit

Potential for preservation of organics

KEYWORDS: Mars, aqueous, water, geochemistry, vein, coating, montmorillonite, smectite, phyllosilicate, sulfate, habitability, organics

Abstract

In the search for evidence of past aqueous activity by the Mars Exploration Rover Opportunity, fracture-filling veins and rock coatings are prime candidates for exploration. At one location within a segment of remaining rim material surrounding Endeavour Crater, a set of "boxwork" fractures in an outcrop called Esperance are filled by a bright, hydrated and highly siliceous (SiO_2~66 wt%) material which has overall a montmorillonite-like chemical composition. This material is partially covered by patches of a thin, dark coating which is sulfate-rich (SO_3~21 wt%) but also contains significant levels of Si, Fe, Ca, and Mg. The simultaneous presence of abundant S, Si, and Fe indicates significant mineralogical complexity within the coating. This combination of vein and coating compositions is unlike previous analyses on Mars. Both materials are heterogeneously eroded, presumably by eolian abrasion. The evidence indicates at least two separate episodes of solute precipitation from aqueous fluids at this location, possibly widely separated in time. In addition to the implications for multiple episodes of alteration at the surface of the planet, aqueous chemical environments such as these would have been habitable at the time of their formation and are also favorable for preservation of organic material.

Introduction

Martian geological formations of chemical sediments can preserve evidence of aqueous activity that cannot occur in the contemporary martian environment because it is too cold and too dry for liquid water or dilute brines to persist at or near the surface. In the exploration of Mars, high priority is placed on discovery of concentrations of salts, clay minerals, and other chemical sediments which can provide evidence for and insight into such past environments and their nature. In some cases, a high concentration of certain elements may provide clues, especially salt-forming elements such as S, Cl, P, C, or N. Clay minerals, many of which are richer in Si than their parent igneous silicate minerals and may also be enriched or depleted in Al, Mg, Fe, or other major elements, are another important indicator of aqueous activity.

Intensive investigations by the Mars Exploration Rover (MER) *Opportunity* in an area called "Matijevic Hill" located on the eastern side of the "Cape York" rim segment of Endeavour Crater resulted in the discovery of "boxwork" (quasi-orthogonal) fractures whose fill material and the coating of the fracture fill are of unique and differing compositions. These materials have compositions which depart from the compositional range of igneous mineral assemblages and are indicators of major aqueous alteration involving non-isochemical processing.

Geologic Setting and Context

Cape York is the informal designation for a segment of the crater rim material surrounding Endeavour Crater at Meridiani Planum, Mars. The rim of this ~22 km diameter crater is discontinuous because of erosion and partial burial by the younger sulfate-rich sandstones of the Burns formation, but a variety of lithologic units have been found in the Cape York segment.

The "Esperance" boxwork is located within the rocks of the Matijevic formation, near the "Whitewater Lake" unit and near where evidence for Fe/Mg smectite was detected from orbit by the CRISM orbiting spectrometer, as described in (Arvidson et al., 2014). The Matijevic formation consists of fine-grained, layered rocks of broadly basaltic composition that contain variable concentrations of spherules of diagenetic or impact origin. These rocks are the only materials identified to date by Opportunity that predate the Endeavour impact (Arvidson et al., 2014).

The boxwork structures (Fig. 1) in the Matijevic formation were analyzed in two separate visits to the area, originally during investigation of another, apparently unrelated, outcrop. Exposed Esperance fracture fill (the "vein") is brighter than either the host rock or its patchy coating, as seen in a mosaic of images acquired by the Microscopic Imager (MI) (Fig. 2). Although definitive mineralogical measurements are no longer possible with the remaining Opportunity payload, it has been reported that this vein material is compositionally congruent with Al-rich smectite (Arvidson et al., 2014; Clark et al. 2014). Here, we derive the detailed chemical compositions of the vein material and the coating, and from those, infer possible mineralogical constituents.

Sampling Strategy

This boxwork fracture system was first studied by the imaging and multispectral visible and near-infrared data from the Panoramic Camera (Pancam), and then analyzed by the Alpha Particle X-ray Spectrometer (APXS) at a location named "Lihir" (Fig. 1), on sol 3239 of the mission timeline. Following rover traverses for investigation of spherules in a nearby location, the operations team decided to return to the boxwork because subsequent analysis of the data showed that Lihir exhibited the lowest Fe and highest Si and Al of any target analyzed during the previous ten year mission by the Opportunity rover at Meridiani Planum.

Stereo imaging data obtained by the MI enabled examination of the microtopography of Esperance, shown in Fig. 3. The general impression from these images is a rugged juxtaposition of flat surfaces having a dark coating at various elevations, separated by areas with no coating. The bright strip of material that runs parallel to the main, coated vein shown in Fig. 3b is actually a steeply inclined sidewall of the overall feature. This strip, visible at the lower right corner, may be the main vein material, stripped of dark coatings and dust, or may be a compositionally-different unit.

In addition to multiple APXS placements to determine changes in overall composition and to assess the relative contributions of vein and other materials, Opportunity's Rock Abrasion Tool (RAT) was used to perform two grindings on Esperance material in an effort to remove as much of the dark coating and soil cover as possible. Significant maneuvering was planned and then accomplished in an effort to optimally position the rover and arm, resulting in partial RAT abrasions at the target location designated Esperance4, on sol 3301 (designated Esperance5) and sol 3305 (Esperance6) (Fig. 5a).

The results of the final grind (Fig. 5b) revealed at least three spherules embedded and partially ground within the vein material. The combined area of these spherules is too small to significantly affect the compositional results from the APXS because of its much larger field of view. For Esperance6, APXS analyses measured the lowest values of FeO and highest values of SiO_2 (see Table 1) so far determined by Opportunity. Some residual, unground patches of coating are evident inside the 45 mm diameter grind circle. Convolving geometric area measurements of 13 patches of coating with an APXS radial response function (R. Gellert, personal communication) that favors material closer to the center of the field of view (FOV) results in the estimation that 9% of the APXS response for this Esperance6 sample is from residual coating material, with the balance from vein surfaces or its powdered grindings. A similar analysis has been performed for the as-is sample, Esperance2, where it is found that the coating is estimated to account for 38% ±4% of the APXS response (this contribution is less certain because of the highly irregular shapes and spotty nature of portions of the coated areas).

Results

Morphology

The MI anaglyph reveals the thinness of the dark coating and its occurrences relative to various portions of vein material (Fig. 3). The MI digital elevation model (DEM) indicates that the coating thickness is not greater than the best depth resolution of the MI, approximately 30 μm. Aeolian physical abrasion or some other process has resulted in a rugged micro-topography from what once may have been a more planar, horizontal surface. The Lihir target (Fig. 4) reveals similar topography and relationships, but lacks the occurrence of the bright strip of vein material. The DEM derived by stereogrammetry (Fig. 3b) also provides evidence that coating material may be physically resistant and has protected the underlying material from aeolian erosion.

Multispectral Imaging

Pancam multispectral imaging of the boxwork before and after RAT grinding provides information relevant to phase (both crystalline and amorphous) assignment. Fig. 6 shows multi-spectral reflectance spectra of RAT-abraded Esperance6 compared with the undisturbed Esperance vein surface and the dark coating. Most importantly, both Esperance bright vein spectra show the 934 to 1009 nm downturn in reflectance indicative of the presence of a hydrated phase (Rice et al., 2010), although the feature is somewhat muted compared to the gypsum veins at Cape York (Farrand et al., 2014)). The dark coating has a Pancam spectrum with no downturn in reflectance, such that a hydrated phase is not indicated. The coating reflectance spectrum is similar to coatings observed on Whitewater Lake (Arvidson et al., 2014), but the detailed compositional profile from APXS is quite different.

Induration

The two RAT grind events each resulted in the same total grind energy of 5.6 J/mm^3. This is a factor of ~10 less than the specific energy expended to grind the Adirondack class basalts on the floor of Gusev crater (S. Indyk, personal communication), a factor of ~50 less than that expended to grind some terrestrial basalts, but approximately the same energy as for grinding gypsum samples during tests in the laboratory (Myrick et al., 2004; Gorevan et al., 2003). The Esperance grind energy places this target in the class of the softer sedimentary materials, as opposed to competent igneous rock. The grind energy is, however, about a factor of 3 to 10 times higher than for grinding the various Burns Formation sediments, and the grind powders are bright grey (Fig. 5a), and lack the red color and strong 535 nm and 865 nm bands of the hematite-laden grinding powders of Burns Formation materials (Clark et al., 2005; Farrand et al., 2007).

Element Trends

Seven APXS measurements, given in Tables 1 and 2, were made at different analysis locations or exposure conditions during the Esperance campaign. A number of well-defined positive and negative trends are apparent in the data. These trends presumably reflect the composition of the dark coating versus the bright vein, as a function of the relative areal proportion of each in the 38-mm diameter FOV of the APXS. That these trends reflect a coating over a material with different composition was confirmed by taking measurements before and after grinding the location designated as Esperance4. Although grinding removed only some of the coating material, some additional areas of coating were obscured with powder from the grinding, resulting in the changes in composition shown in Fig. 7. Removing and obscuring the coating resulted in less S, Fe, Ca, and Mg. Exposing more vein material for analysis produced sharp increases in Si and Al.

The trends that are observed for the various APXS placements and grindings at Esperance are less ambiguous than is often the case for in situ measurements on Mars and permits a quantitative unmixing model approach to the analysis. Many major elements correlate negatively with SiO_2 concentration, while only Al clearly correlates positively (Fig. 8). Extrapolations of S, Fe, and Ca trends implicate a theoretical end member approaching ~70 wt% SiO_2 in composition. The Al correlation is expanded in Fig. 9 to show a predominant trendline that intersects the axis at ~ 26 wt% SiO_2. For the coating end-member, a value of ~21 wt% SO_3 is found when extrapolating to zero Al_2O_3.

One minor element, Cr, follows Si closely (Fig. 10). The slope of the least-squares trendline gives a ratio of $Cr_2O_3/SiO_2 = 0.0048$ (wt/wt), which normally ranges from 0.0047 to 0.0060 for the majority of rocks and sediments analyzed at Meridiani, including the Burns Formation sandstones (Clark et al., 2005), although it is somewhat higher in soils, and about twice this value in Gusev basalts (Gellert et al., 2004). This correlation could indicate that Cr-bearing accessory mineral(s) resisted the alteration processes that concentrated Si, analogous to the chromite in the “Assemblée” outcrop on Husband Hill in Gusev Crater which overall also has an Al- and Si-rich, Fe-poor, montmorillonite-like chemical composition (Clark et al., 2007).

Chromium is commonly enriched in the clay fractions of sediments (Ilton, 1999). Although Ti can also be concentrated in residual phases in aqueous alteration settings, the plot shows that Ti has no clear trend with Si (or with Fe).

Many elements trend in a strongly positive direction with Fe or S, which also trend strongly with one another. The formal statistical correlations are summarized in Fig. 11, where it is seen that no less than 8 elements follow one-another, the most prominent of which are Fe, S, Ca, and Mg. Two trace elements, Br and Zn, show uncommonly high correlation and consistent trends with S (Fig. 11 and 12).

As seen in the bar chart of Fig. 13, the concentration of S significantly decreased as grinding progressed, but Cl is approximately the same for all Esperance targets, irrespective of the relative proportions of vein material and coating. These results indicate that there must be Cl in both coating and vein, at a level of about 2.5 wt% in each, which is five times higher than the Cl in martian universal soils (Yen et al., 2005). The Lihir sample does contain less Cl, however, so there could be some variability in Cl depending on location within the boxwork vein system itself. Interestingly, the Na/Cl (atom/atom) ratio is near unity (1.02 ± 0.18) in all occurrences. This could imply the presence of Na chloride, or any of its oxidized forms, such as perchlorates, chlorates, etc. (Kounaves et al., 2014).

Methodology for Calculating Compositions

From the coating fractional coverage and calculated APXS responses, relative to the vein x-ray response, given in the Sampling Strategy section above, it is possible to directly calculate compositions for the coating and vein material from the Esperance2 and Esperance6 measurements alone.

We then verified that the two compositional profiles (vein and coating) could explain all measurements taken at Lihir and Esperance locations by choosing a fraction of coating for each sample. Best-fit areal fractions were derived by minimizing errors for four major elements (SO_3, SiO_2, FeO and Al_2O_3). We found that all other elements were then predicted at or near their measured values. The largest deviations were the Cl and Na_2O concentrations, which are especially different for the Lihir sample. .

For some elements (Na, P, Cl, Ti, and Ni), the concentrations are the same, or approximately so, in both coating and vein, as evidenced by only small variations in their concentrations (Table 2). No direct information is available on Fe^{2+}/Fe^{3+} ratios for these measurements (although Pancam measurements of 535 nm band depth, which Farrand et al. (2006, 2008) found to correlate with Moessbauer Fe^{3+}/Fe_{Total}, are higher for the coating than for the vein). At this time, all values for Fe are given in terms of the traditional reporting by APXS for total Fe as FeO.

The resulting chemical compositions are provided in Table 1 and in pie charts (Fig. 14 and 15).

As noted above, the MI analysis indicates the coating is very thin, possibly less than 100 µm thick. Detailed calculations using standard x-ray cross-section data (NIST, 2011) and inferred compositions show that while the x-rays from Mg through Ca originate from the topmost 2 to 30 µm of the coating, the Fe can originate much deeper. Consequently, the true composition of the coating could be higher in FeO by about 10% (relative) if the thickness of the coating is 100 µm, and could be as much as twice its apparent concentration if the coating is actually only ~30 µm thick. This is because the Fe K-alpha fluorescent x-ray (6.4 keV) can penetrate this coating much more efficiently than Ca, S, and especially Si and Mg (1.25 keV) primary fluorescent x-rays. If very thin, the excitation source's x-rays mostly pass through the coating into the underlying vein material. The coating would not allow Si or Al signals from the vein to pass back to the detector, however, because even 5 µm of coating would strongly attenuate the low-energy x-rays from these elements.

In contrast to a uniform sample, a thin coating likely cannot be assessed for its very light element content (O, C, N, H) by APXS because the technique involves the use of the high energy Pu x-rays from the radiation source. These highly penetrating x-rays would easily pass through a thin coating and are scattered preponderantly by the vein and hence confound the detection (or lack thereof) of light elements in the coating itself.

The inaccuracies in the element concentrations in the coating are much higher than for the vein material for several reasons: (1) no APXS analysis target had much more than ~1/3 of its coating within the most sensitive portion of its FOV, whereas the Esperance6 sample had 91% of vein material comprising the x-ray response; (2) the coating is chemically more complex than the vein material; (3) the coating could only be measured on "as-is" samples, which may also have aeolian-deposited dust partially skewing the composition; and (4) there are uncertainties in the actual thickness of the coating, which could affect the x-ray analysis.

Discussion

From these results, the possible mineralogical components and constraints upon their formation may be assessed. Either material, vein fill or coating, might be amorphous or contain amorphous components. Although definitive mineralogical data is lacking, the compositional and other data allow assessments of the plausible mineralogical make up of these two materials. The simpler composition of vein material is more amenable to such assessments.

Mineralogical Candidates for Vein Material

Interpretation of the chemical composition of the vein material as a putative montmorillonite hinges on its brightness, hydration state, and especially its elemental profile. Multiple minerals might combine to give the same or similar net chemical composition. However, the ratio of Al to Si in the vein material corresponds to 0.30 (atom/atom), which is somewhat below the typical range for montmorillonite (Al/Si of 0.37 to 0.5, Grim and Güven, 1978). In contrast, however, many families of clay minerals and mineraloids are much more aluminous: kaolinite and halloysite have Al/Si=1.0; beidellite is ~ 0.7; allophanes range from 1.0 to 1.5, imogolite is 2.0, and chlorites are also too high at 0.67. Furthermore, many clay minerals contain larger amounts of cations such as Na, Mg, Fe, or Ca, all of which are at very low abundance in this vein material.

The alkali feldspars have low Al/Si (0.33) but anorthite is too high (1.0). In addition, all feldspars require cations such as Ca, Na, and/or K, at levels that are not present, as Fig. 11(B) of Arvidson et al. (2014) illustrates.

Certain zeolites can have similar elemental components as montmorillonites and are candidate minerals on Mars from alteration of basalt (Ming et al., 2007). Most zeolites, however, such as phillipsite, analcime, natrolite, prehnite, or stilbite, contain significant levels of essential Na_2O, K_2O or CaO which are far higher, totaling 10 to 28 wt% (Cloutis et al., 2002)), than the total concentrations of these elements (3.5 wt% total) in the Esperance vein material. Also, in many cases their Al/Si ratios are either too high or too low. Analysis of orbital remote sensing for possible martian zeolites (Wray et al., 2009; Carter et al., 2013) point out the difficulties in confirming detections because of band overlaps with spectral features of sulfates.

The bar chart plot of Fig. 17, shows that the composition of the vein material corresponds generally to the natural range of terrestrial montmorillonites, as also does the Independence class of putative montmorillonite material on Husband Hill in Gusev crater (Clark et al., 2007). Because the Al/Si ratio is somewhat low, the Esperance vein material would be more in-family with terrestrial montmorillonites if it included a siliceous component. Silica has been identified in soils on Husband Hill and near Home Plate, either in near-pure form or in some cases associated with sulfate salts (Wang et al., 2008; Yen et al., 2008). The indication of a silica phase, possibly hydrated, in Esperance vein composition was previously reported (Arvidson et al., 2014). Here, we find that allocating between one-sixth and one-fourth of the analyzed SiO_2 to silica would result in a composition for the remaining component that fits wholly within the range of the montmorillonites shown in Fig. 16. Other siliceous alteration products such as the smectite clay minerals hectorite (a Mg-Si clay mineral) and hisingerite (Fe-Si), could be minor accessory phases that contribute Si.

Also potentially relevant is that in studies of the acid sulfate alteration of smectites, Altheide et al (2010) demonstrated the leaching of Al from montmorillonite to produce amorphous silica. The Esperance vein material could thus be the product of acidic diagenesis of montmorillonite (or its precursor).

In terrestrial settings, illite is often found located nearby, and can be interbedded or even interlayered with montmorillonites. However, illite contains ~ 7 wt% K_2O. What little K_2O occurs in the Esperance6 RAT sample (0.24 wt%) correlates with the coating much better than with the vein. Thus, there is no tangible evidence for the presence of illite or any other phase with comparable or higher K_2O concentrations as an accompanying mineral in the vein material.

It is often noted by clay mineralogists that Mg can aid the formation of montmorillonites (e.g., Grim and Güven, 1978). Element trends indicate that Mg is reasonably abundant in both the vein and coating. Grim and Kulbicki (1961) discriminate between cheto and wyo types of montmorillonite, whose physical properties differ somewhat and whose end-member Mg/Al (atom/atom) ratios are 0.39 and 0.09, respectively (see also Alberti and Brigatti, 1985). The corresponding Mg/Al ratio for the vein is 0.31 (atom/atom), which is more cheto-like than wyo-like, as was also the case for the Assemblée (0.38) outcrop at Gusev crater (Clark et al., 2007).

Mineralogical Candidates for Coating Material

Assessment of the types of phases within the coating is also challenging, not only because of some uncertainties in element concentrations, but also because of multiple major elements not commonly found together in terrestrial analogs. It should be noted, however, that Fe sulfates discovered on Husband Hill in Gusev Crater also have, like this coating material, high Si with low Al, as well as significant levels of Mg and Ca.

Each of the abundant Mg, Ca, and Fe cations could be present as sulfates, silicates, or both. The concentration of Ca in the coating is close to but not quite enough to accommodate all the SO_3 solely as $CaSO_4$. As seen in figure 14, the trend line for CaO vs SO_3 passes through the origin and has a slope of 0.60, somewhat less than the stoichiometric slope of 0.70 for $CaSO_4$, indicating that if most or all of the Ca is in the salt, there must be at least one other cation associated with the sulfate. The level of Mg would have been adequate to explain all SO_3 as $MgSO_4$ but the trend plot shows that Mg occurs in both materials and the Fe concentration is more than sufficient for all SO_3 to be an iron sulfate, but the Fe commonly occurs also in other minerals. All three of these sulfates have been found in high concentration at various locations on Mars (e.g., Morris et al., 2006, 2008; Yen et al., 2008). Sulfates of Mg, Ca, or Fe^{3+} are generally white to yellow, not dark, and have been observed in these colorations on Mars. However, ferrous sulfate can be dark, especially if anhydrous.

The silicates could include mafic minerals or amorphous materials. The Mg-Fe-Si content cannot be simply explained with an olivine source, as there are inadequate mafic elements relative to Si (unless, of course, the Fe is actually much higher than analyzed, due to coating thinness). A pyroxene source is reasonable: the native minerals can be dark, and their derived products can be as well. There could be any number of potential Fe oxides and/or oxyhydroxide phases -- e.g., hematite, magnetite, goethite, and/or npOx, among the large set of Fe minerals that has already been discovered on Mars (Morris et al., 2006, 2008). Some of these oxides can be very dark. Various combinations of Fe-Mg-Ca carbonates as secondary alteration products have been found in martian meteorites (e.g., Velbel, 2012). Morris et al. (2010) report that the Comanche outcrop contains one-third carbonate by volume, predominantly as Mg (and Mn-bearing) but also with significant Fe and Ca.

Smectites such as saponite or nontronite are generally lighter-toned, although their colors may vary considerably depending upon accessory minerals. Furthermore, these smectites commonly contain some amount of Al and much higher Si than the coating.

Regardless of the detailed mineralogy, the Esperance dark coating is quite distinct in chemical composition from the nearby Mg-Fe smectites implicated in dark coatings on the “Sandcherry” rocks (Arvidson et al., 2014) which contain, for example, 9 wt% Al_2O_3, whereas the Esperance coatings contain virtually none. Similarly, the Esperance coating material cannot simply be soil or the amorphous component in soil (Morris et al., 2015; Blake et al., 2013) with some added salts because these other materials have significant Al_2O_3 (e.g., 6 - 10 wt%) and only 7 – 9 wt%

MgO and 4 – 8 wt% CaO. In any case, aqueous processes are indicated for coating formation because of its distinctive composition, even though the styles and resulting mineralogies cannot be conclusively determined.

Implications

Aqueous Processes and Conditions

On Earth, montmorillonites and silica result from aqueous alteration of igneous rocks and basaltic glasses, but can form by a variety of pathways. The most common origin of highly concentrated quantities of montmorillonite is from in situ alteration of volcanic ash or tuff deposits under poorly drained, alkaline conditions with availability of Mg (Gaines et al., 1997; Grim and Güven, 1978; Ross and Hendricks, 1945). Translocation from the original deposit can relocate the material to form a separate bed or deposit.

Interestingly, although the vein material has a low concentration of Fe, the relative concentration of Mn (inferred to be ~7 atoms Mn /100 atoms of Fe) is among the highest that has been found in Meridiani Planum, and significantly higher than for the Azilda (2.4 atoms/100 atoms Fe) and Amboy (4.6) rocks nearby (Arvidson et al., 2014). It is also ~ 3 times higher than the Independence or Assemblee outcrops (Clark et al., 2004). Even greater Mn enrichments have been reported recently, discovered underneath surfaces on the Pinnacle Island and Stuart Island rocks (Farrand et al., 2014; Arvidson et al., this volume) at Cook Haven, in the adjacent rim segment of Endeavour Crater, and for certain rocks in Gale crater by the Curiosity rover (Lanza et al., 2014). For this vein silicate, the higher Mn/Fe is a likely indicator that aqueous processing was under conditions that favored Mn dissolution over Fe extraction, as primary sources with such high Mn/Fe have not been observed. For example, from the Pourbaix diagrams for Mn and Fe stability fields, there is a band of Mn solubility where Fe precipitates whenever the oxidation potential (Eh) exceeds a critical value, which increases as pH becomes lower (Atkins et al., 2010).

In contrast, the concentration of Mn relative to Fe in the boxwork dark coating is close to the ratio found in soils, rocks, and the Burns Formation sediments, namely, in the range of 2 to 2.5 atoms of Mn per 100 atoms Fe. Manganese is generally more easily mobilized than Fe, but likewise not so readily precipitated from solution unless the environmental pH and/or Eh are substantially changed. If the coating solution was leached from soils or from typical Meridiani rocks under conditions that favored solubilization of both elements, and then precipitated by quantitative evaporation or freezing, the original Mn/Fe ratio could be preserved, such as is observed in the coating. For the vein silicates, the higher Mn/Fe may be a tracer for the original source material (e.g., Amboy-like rather than Azilda-like).

Multiple Aqueous Episodes

The existence of a dark coating indicates an episode that post-dates the formation of the vein fracture filling material itself. If so, the contemporary vein and coating can be explained by two separate and independent aqueous episodes, with no obvious constraints on the length of the time interval between them. Alternatively, a major change toward the end of a single event, such as a change in solution temperature or chemical composition, might cause an evolution in composition that results in the differences between top surface and the bulk material, but there is no evidence of gradation in the samples.

The thinness of the dark coating could be indicative of a relatively short-term aqueous event whereby a salt-rich solution precipitated its contents. Without all the tools and techniques available for laboratory analyses, we cannot preclude the possibility of multiple diagenetic processes that altered the coating over time. The indications of multiple mineral component phases (sulfates, oxides, and silicates), each with different solubility functions, add plausibility to this possibility.

The cm-scale width of the bright fracture filling material indicates the likelihood of a long term pervasive build-up of material. As with fracture fillings on Earth, it would be rare to occur in one short episode, and would more likely proceed as repeated precipitation from solution or else progressive alteration of the walls of the host rock. Furthermore, if the availability of liquid H_2O was variable, the well-known expansive nature of the smectite clays may have provided lateral forces for enlargement of the fracture itself. Montmorillonite swelling as a result of wetting after contraction during desiccation can produce pressures reaching 0.5 to 10 MPa, depending on exchange cations, density, and degree of wetting (Pusch and Yong, 2005). Pressure fracturing by wetting and subsequent shrinkage by desiccation could create additional channels for subsequent cycles of flow. These pressures due to expansions could also force protrusion of material above the local surface. Freezing of clay when in the form of a gel, with subsequent desiccation to remove interstitial H_2O, typically produces low-density, weaker material. However, the resistance to grinding of such material would be far less than that observed for the RAT grinding of Esperance.

An important ambiguity is whether the dark coating material would be susceptible to removal by dissolution if exposed to liquid water. Many coatings, such as metal skins, desert varnish, or carbonate deposits, can be built up as precipitates from liquid films and then become resistive to further dissolution via oxidation and/or other forms of consolidation or “case hardening” of their constituents (Dorn, 1998), possibly enhanced by the extreme UV and highly oxidative photochemical products in the martian atmosphere. The dark coating’s apparent long-term, albeit patchy, survival against aeolian abrasion is an indirect indicator of its strength and degree of induration. Indeed, as seen in the anaglyphs (Fig. 3 and Fig. 4), the coating often caps high points in topography, indicative of protection of vein material against erosion.

The origin of this boxwork may be related to the formation of Endeavour Crater. This hypervelocity impact would have produced substantial fracturing as well as injecting a large amount of heat energy into the subsurface, resulting in hydrothermal activity if ice or hydrated minerals were present. Such activity could persist until the thermal die-away was complete or the supply of volatiles was exhausted (Newsom, et al. 2001).

Additional High-Si Occurrences

The vein material in the Esperance boxwork has many similarities to the Independence and Assemblée outcrops on Husband Hill in Gusev crater, especially in the high Al/Si ratio and low abundance of Fe and other cations. Other high-Si occurrences near Home Plate in the Columbia Hills of Gusev crater (KenoshaComets and FuzzySmith, as analyzed by the MER Spirit rover) have significant differences in composition (Table 3), although they share the 934 to 1009 nm drop in reflectance seen in the Pancam spectra (Rice et al., 2010). Clearly, the details of formation and outcomes are different, even though the end result is enrichment in Si through H_2O-mediated alteration processes. The two targets with putative montmorillonite -- Independence and Esperance -- have high Al/Si ratios, but distinctly different Cr and Ti abundances, indicating differences in source material or physical and chemical pathways to the end product. Independence also has accessory phosphate and trace elements, whereas Esperance vein material does not.

Astrobiological Significance

In the early history of Mars, there were periods in time and certain regional locations for which the environment was far more conducive to the flourishing of various forms of life, as evidenced by geomorphological landforms created by flowing water as well as deposits of chemical sediments. Much of this evidence comes from observations on large scales, as obtained by remote sensing by orbital missions. Exploration on the ground has shown, however, that many additional loci of favorable environmental niches were present in past epochs, even though evidence of such environmental niches from the global surveys may be scant or lacking. Such dispersed, local refuges could have been accessed by a global biota through passive dispersal of microorganisms by aeolian transport, just as rare, isolated deep sea hydrothermal vents become populated by fluid transport of organisms from one favorable locale to the next. We argue that Esperance could be one such example.

Formation of montmorillonite and associated clay minerals of similar composition generally occurs at pH values in the range of neutral to mildly alkaline conditions (Gaines et al., 1997; Grim and Güven, 1978). Terrestrial taxa which can flourish under such conditions are among the most common and most widespread on Earth. Because clay minerals can serve as reservoirs of exchangeable cations, they help concentrate and make bioavailable many essential trace elements important for the most efficient function of a variety of metabolic activities. Although clay minerals may ultimately compete for the uptake and sequestration of scarce water resources, their initial formation conditions are an indicator for water/rock ratios favorable to biological function. Alkaline conditions are also favorable to a broad range of abiotic chemical reactions for forming the building block molecules needed for the emergence of life, whereas acidic environments are unfavorable (Knoll et al., 2005). Clay minerals and especially montmorillonite are also often invoked as stabilizers or catalysts for abiotic chemical evolution (Bernal, 1951;

Hashizume, 2012) which could lead to life, including polymerization of RNA (e.g., Ferris et al., 1996; Joshi et al., 2011) and catalyzes formation of organic vesicles (Hanczyc et al., 2003). In addition, the source region for the fluids that deposited their siliceous content into the fracture system may have had different physicochemical conditions, providing an additional, separate habitable environment.

Coatings of various types are well known loci for lithobiotic activity on the microscale (Chan et al, 2013; Dorn, 1998). Examples range from carbonate crusts to iron oxyhydroxide coatings, from nitrates to desert varnishes, and from silica glazes to metal skins (Dorn, 1998). The Esperance coating is dark and metal-ion-rich, providing a strong natural absorber of short-wavelength UV to protect organic material or endolithic organisms in the interior of the coating as well as in the vein material it overlies. The low albedo also facilitates warming during daytime. Capability to capture ambient H_2O is uncertain, but the relatively high Cl content of both vein and coating may implicate unusually high concentration of perchlorate salts with strong deliquescence and freezing point depression properties, apparently widespread on Mars (Kounaves et al., 2014; Leshin et al., 2014; Clark and Kounaves, 2015; Ojha et al., 2015).

Both salts and clay minerals have been identified as favorable to the long-term preservation of organic matter (Summons et al., 2011), although oxychlorines are not (Kounaves et al., 2013). The coating itself, however, is directly exposed to all the debilitating components of the environment which can destroy organics, such as extreme UV, atmospheric oxidants including photochemical products, and energetic solar flare protons.

Acknowledgements

Digital data not presented in numerical form in this paper can be accessed through the NASA Planetary Data System Geosciences Node (http://pds-geosciences.wustl.edu/).

We are indebted to NASA for their support, including the Jet Propulsion Laboratory and the many engineers and supporting scientists who have enabled continuation of the highly productive mission and discoveries of the MER Opportunity rover. Early recognition of the potential importance of the boxwork was championed by S. W. Ruff, and we thank him also for comments on an early draft of the manuscript.

References Cited

Alberti, A., and Brigatti, M.F. (1985) Crystal chemical differences in Al-rich smectites. Clays and Clay Minerals, 33, 546-558.

Arvidson, R.E., Squyres, S.W., Bell III, J.F., Catalano, J. G., Clark, B. C., Crumpler, L. S., de Souza Jr., P. A., Fairén, A. G., Farrand, W. H., Fox, V. K., Gellert, R., Ghosh, A., Golombek, M. P., Grotzinger, J. P., Guinness, E. A., Herkenhoff, K. E., Jolliff, B. L., Knoll, A. H., Li, R., McLennan, S. M., Ming, D. W., Mittlefehldt, D. W., Moore, J. M., Morris, R. V., Murchie, S. L., Parker, T. J., Paulsen, G., Rice, J. W., Ruff, S. W., Smith, M. D., and Wolff, M. J. (2014) Ancient aqueous environments at Endeavour Crater, Mars. Science, 343, 1-8 (DOI:10.1126/science.1248097)

Atkins, T., Overton, T., Rourke, J., Weller, M., and Armstrong, F. (2010) Inorganic Chemistry, 5th Edition. Oxford University Press.

Altheide, T.S., Chevrier, V.F., and Dobrea, E.N. (2010) Mineralogical characterization of acid weathered phyllosilicates with implications for secondary martian deposits. Geochimica et Cosmochimica Acta, 74, 6232-6248. doi:10.1016/j.gca.2010.08.005

Bernal, J. D (1951) The Physical Basis of Life. London: Routledge and Kegan Paul. 364p.

Blake, D. F., Morris, R. V., Kocurek, G., Morrison, S. M., Downs, R. T., Bish, D., Ming, D. W., Edgett, K. S., Rubin, D., Goetz, W., Madsen, M. B., Sullivan, R., and 400 others (2013) Curiosity at Gale Crater, Mars: Characterization and analysis of the Rocknest sand shadow. Science, 341, DOI: 10.1126/science.1239505.

Carter, J., F. Poulet, Bibring, J.-P., Mangold, N., and Murchie, S. (2013) Hydrous minerals on Mars as seen by the CRISM and OMEGA imaging spectrometers: Updated global view. Journal of Geophysical Research: Planets, 118, 831–858, doi:10.1029/2012JE004145.

Chan, Yuki, Van Nostrand, J.D., Zhouc, J., Pointinga, S. B., and Farrell, R. L. (2013) Functional ecology of an Antarctic dry valley. Proceedings of the National Academy of Science (PNAS) 110, 8990–8995, doi: 10.1073/pnas.1300643110

Clark, B.C., and Kounaves, S. P. (2015) Evidence for the distribution of perchlorates on Mars. International Journal of Astrobiology, in press.

Clark, B. C., Arvidson, R., Gellert, R., Morris, R. V., Ming, D. W., Richter, L., Ruff, S., Michalski, J.,m Farrand, W., Herkenhoff, K., Li, R., Squyres, S. W., Yen, A., and Schröder, C. (2007) Evidence for montmorillonite or its compositional equivalent in Columbia Hills, Mars. Journal of Geophysical Research, 112, 1-19. doi:10.1029/2006JE00., 2007.

Clark, B. C., Morris, R. V., McLennan, S. M., Gellert, R., Jolliff, B., Knoll, A. H., Squyres, S. W., Lowenstein, T. K., Ming, D. W., Tosca, N. J., Yen, A., Christensen, P. R., Gorevan, S., Brückner, J., Calvin, W., Dreibus, G., Farrand, W., Klingelhoefer, G., Waenke, H., Zipfel, J., Bell, J. F., Grotzinger, J., McSween, H. Y., and Rieder, R. (2005) Chemistry and mineralogy of outcrop at Meridiani Planum, Mars. Earth and Planetary Science Letters, 240, 73-94.

Clark, B. C., Gellert, R., Arvidson, R. E., Squyres, S. W., Ruff, S. W., Herkenhoff, K. E., Jolliff, B.and Yen, A. S. (2014) Esperance: Extreme aqueous alteration in fracture fills and coatings at Matijevic Hill, Mars. Lunar and Planetary Science Conference, Extended Abstracts #1419.

Gellert, R., Rieder, R., Anderson, R. C., Brückner, J., Clark, B. C., Dreibus, G., Economou, T., Klingelhöfer, G., Lugmair, G. W., Ming, D. W., Squyres, S. W., d'Uston, C., Wänke, H., Yen, A., and Zipfel, J. (2004) Chemistry of rocks and soils in Gusev Crater from the Alpha Particle X-ray Spectrometer. Science, 305, 829-832, DOI: 10.1126/science.1099913.

Cloutis, E.A., Asher, P. M. , and Mertzman, S. A. (2002) Spectral reflectance properties of zeolites and remote sensing implications. Journal of Geophysical Research, 107, doi: 10.1029/2000JE001467.

Dorn, R.I. (1998) Rock Coatings (Developments in Earth Surface Processes). Elsevier, 444 pp., ISBN-13: 978-0444829191.

Ehlmann, B. L., Mustard, J. F. , Murchie, S. L., Bibring, J-P., Meunier, A., Fraeman, A. A., Langevin, Y. (2011) Subsurface water and clay mineral formation during the early history of Mars. Nature, 479, 53-60. doi:10.1038/nature10582

Farrand, W.H., Bell III, J.F., Johnson, J.R., Squyres, S.W., Soderblom, J., and Ming, D.W. (2006) Spectral variability among rocks in visible and near infrared multispectral Pancam data collected at Gusev Crater: Examinations using spectral mixture analysis and related techniques. Journal of Geophysical Research: Planets, 111, E02S15, 10.1029/2005JE002495

Farrand, W.H., Bell III, J.F., Johnson, J.R., Arvidson, R.E., Crumpler, L.S., Hurowitz, J.A., and Schröder, C. (2008) Rock spectral classes observed by the Spirit rover's Pancam on the Gusev crater plains and in the Columbia Hills. Journal of Geophysical Research, 113, E12S38, doi:10.1029/2008JE003237

Farrand, W.H., Bell III, J.F., Johnson, J.R., Rice, M.S., Jolliff, B.L., and Arvidson, R.E. (2014) Observations of rock spectral classes by the Opportunity rover's Pancam on northern Cape York and on Matijevic Hill, Endeavour Crater, Mars. Journal of Geophysical Research:. Planets, 119, doi:10.1002/2014JE004641.

Farrand, W.H., Bell III, J.F., Johnson, J.R., Joliff, B.L., Knoll, A.H., McLennan, S.M., Squyres, S.W., Calvin, W.M., Grotzinger, J.P., Morris, R.V., Soderblom, J., Thompson, S.D., Watters, W.A., and A.S. Yen (2007) Visible and near-infrared multispectral analysis of rocks at Meridiani Planum, Mars by the Mars Exploration Rover Opportunity. Journal of Geophysical Research: Planets, 112, E06S02, 10.1029/2006JE002773

Ferris J.P., Hill, A.R. Jr, Liu, R., and Orgel, L.E. (1996) Synthesis of long prebiotic oligomers on mineral surfaces. Nature. 381, 59-61.

Gaines, R.V., Skinner, H. C. W., Foord, E.E., Mason, B., and Rosenzweig, A. (1997) Dana's New Mineralogy. J. Wiley and Sons, New York.

Gorevan, S. P., Myrick, T. M., Davis, K., Chau, J. J., Bartlett, P., Mukherjee, S., Anderson, R., Squyres, S. W., Arvidson, R. E., Madsen, M. B., Bertelsen, P., Goetz, W., Binau, C. S., and Richter, L., (2003) Rock Abrasion Tool: Mars Exploration Rover mission. Journal of Geophysical Research, 108, E12, 2003, pp. 9-1 – 9-8.

Grim, R.E., and Kulbicki, G. (1961) Montmorillonite: high temperature reactions and classification. American Mineralogist, 46, 1329-1369.

Grim, R.E., and Güven, N. (1978) Bentonites: Geology, mineralogy, properties and uses. Elsevier Sci. Publ. Co., Amsterdam.

Hanczyc, M. M., Fujikawa, S. M., and Szostak, J. W. (2003) Experimental models of primitive cellular compartments: Encapsulation, growth, and division. Science, 302, 618-622. (DOI:10.1126/science.1089904)

Hashizume, Hideo. (2012) Role of clay minerals in chemical evolution and the origins of life. In Valaskova, Marta, Ed., Clay Minerals in Nature - Their Characterization, Modification and Application.. ISBN: 978-953-51-0738-5, InTech, DOI: 10.5772/50172.

Ilton, E.S. (1999) Chromium, in Marshall and Fairbridge (1999).

Joshi P. C., Aldersley, M. F., and Ferris, J. P. (2011) Progress in demonstrating total homochiral selection in montmorillonite-catalyzed RNA synthesis. Biochemical and Biophysical Research Communications, 413, 594-8. doi: 10.1016/j.bbrc.2011.09.008.

Knoll, Andrew H., Carr, Michael, Clark, Benton, Des Marais, David J., Farmer, Jack D., Fischer, Woodward W., Grotzinger, John P., McLennan, Scott M., Malin, Michael, Schröder, Christian, Squyres, Steven, Tosca, Nicholas J., Wdowiak, Thomas. (2005) Astrobiological implications of Meridiani sediments.Earth and Planetary Science Letters, 240, 179-189.

Kounaves, S. P., Carrier, B. L., O'Neil, G. D.. Stroble, Sh. T., and Claire, M. W. (2013) Destruction of organics on Mars by oxychlorines: Evidence from Phoenix, Curiosity, and EETA 79001. European Planetary science Congress (EPSC) Extended Abstracts, EPSC2013, 8, 799-1.

Kounaves, S. P., Chaniotakis, N. A., Chevrier, V. F., Carrier, B. L., Folds, K. E., Hansen, V. M., McElhoney, K. M., O'Neil, G. D., and Weber, A. W. (2014) Identification of the perchlorate parent salts at the Phoenix Mars landing site and possible implications. Icarus, 232, 226-231, doi:10.1016/j.icarus.2014.01.016.

Lanza, N. L., Ollila, A. M., Cousin, A., Hardgrove, C., Wiens, R. C., Mangold, N., Nachon, M., Fabre, C., Bridges, N., Johnson, J., Le Mouelic, S., Cooper, D., Schmidt, M., Berger, J., Bell, J., Arvidson, R., Mezzacappa, A., Jackson, R., Clegg, S., Clark, B., and 12 others (2014) Manganese trends with depth on rock surfaces in Gale Crater, Mars. Lunar and Planetary Science Conference, Extended Abstracts #2599.

Leshin, L. A., Mahaffy, P. R., Webster, C. R., Cabane, M., Coll, P., Conrad, P. G., Archer, P. D., Atreya, S. K., Brunner, A. E., Buch, A., Eigenbrode, J. L., Flesch, G. J., Franz, H. B., Freissinet, C., Glavin, D. P., McAdam, A. C., Miller, K. E., Ming, D. W., and 428 others. (2013) Curiosity Rover volatile, isotope, and organic analysis of Martian fines. Science, 341. DOI: 10.1126/science.1238937.

Marshall, C.P., and Fairbridge, R.W. (1999) Encyclopedia of Geochemistry. Kluwer Academic Publications, Great Britain.

Martin M., Hanczyc, S. M., Fujikawa, M., and Szostak, J. W. (2003) Experimental models of primitive cellular compartments: Encapsulation, growth, and division. Science, 302, 618-622. (DOI:10.1126/science.1089904)

Ming, D. W., Morris, R. V., and Clark, B. C. (2007) The Martian Surface: Composition, mineralogy, and physical properties. In Bell III, J.F., Ed., Cambridge University Press, 2007.

Morris, R. V., Klingelhöfer, G., Schröder, C., Rodionov, D. S., Yen, A., Ming, D. W., de Souza Jr., P. A., Fleischer, I., Wdowiak, T., Gellert, R., Bernhardt, B., Evlanov, E. N., Zubkov, B., Foh, J., Bonnes, U., Kankeleit, E., Gütlich, P., Renz, F., Squyres, S. W., and Arvidson, R. E. (2006) Mössbauer mineralogy of rock, soil, and dust at Gusev Crater, Mars: Spirit's journey through weakly altered olivine basalt on the Plains and pervasively altered basalt in the Columbia Hills. Journal of Geophysical Research, 111, E02S13, doi:10.1029/2005JE002584.

Morris, R. V., Klingelhöfer, G., Schröder, C., Fleischer, I., Ming, D. W., Yen, A. S., Gellert, R., Arvidson, R. E., Rodionov, D. S., Crumpler, L. S., Clark, B. C., Cohen, B. A., McCoy, T. J., Mittlefehldt, D. W., Schmidt, M. E., de Souza Jr., P. A., and Squyres, S. W. (2008) Iron mineralogy and aqueous alteration from Husband Hill through Home Plate at Gusev Crater, Mars: Results from the Mössbauer instrument on the Spirit Mars Exploration Rover. Journal of Geophysical Research, 113, E12S42, doi:10.1029/2008JE003201.

Morris, R.V., Ruff, S. W., Gellert, R., Ming, D. W., Arvidson, R. E., Clark, B. C., Golden, D. C., Siebach, K., Klingelhöfer, G., Schröder, C., Fleischer, I., Yen, A. S., and Squyres, S. W. (2010) Identification of carbonate-rich outcrops on Mars by the Spirit Rover. Science, 329, 421-424. DOI: 10.1126/science.1189667.

Myrick, T. M., Bartlett, P., Carlson, L., Chu, P., Davis, K., Chau, J., Powderly, J., and Wilson, J. (2004) The RAT as a rock physical properties tool. AIAA 2004-6096, Space 2004 Conference, San Diego, CA, USA.

Newsom, H.E., Hagerty, J.J., and Thorsos, I.E. (2001) Location and sampling of aqueous and hydrothermal deposits in Martian impact craters. Astrobiology, 1, 71-88.

NIST (2011) XCOM: Photon Cross Sections Database. NIST Standard Reference Database 8 (XGAM), http://www.nist.gov/pml/data/xcom/.

Ojha, L., Wilhelm, M.B., Murchie, S.L., McEwen, A.S., Wray, J.J., Hanley, J., Massé, M., and Chojnacki, M. (2015) Spectral evidence for hydrated salts in recurring slope lineae on Mars. Nature Geoscience, 8, 829–832. doi:10.1038/ngeo2546.

Pusch, R., and Yong, R.N. (2005) Microstructure of smectite clays and engineering performance. CRC Press, ISBN-13: 9780203028988

Rice, M.S., Bell III, J.F., Cloutis, E.A., Wang, A., Ruff, S.W., Craig, M.A., Baily, D.T., Johnson, J.R., de Souza Jr., P.A., and Farrand, W.H. (2010) Silica-rich deposits and hydrated minerals at Gusev crater, Mars: Vis‐NIR spectral characterization and regional mapping. Icarus, 205, 375–395.

Ross, C.S., and Hendricks, S.B. (1945) Minerals of the montmorillonite group: Their origin and relation to soils and clays. U.S. Geological Survey Professional Paper 205B.

Summons, Roger E., Amend, Jan P., Bish, David, Buick, Roger, Cody, George D., Des Marais, David J., Dromart, Gilles, Eigenbrode, Jennifer L., Knoll, Andrew H., and Sumner, Dawn Y. (2011) Preservation of Martian organic and environmental records: Final Report of the Mars Biosignature Working Group. Astrobiology, 11, 157-181. DOI: 10.1089/ast.2010.0506

Velbel, M.A. (2012) Aqueous alteration in Martian meteorites: Comparing mineral relations in igneous-rock weathering of Martian meteorites and in the sedimentary cycle of Mars. In Grotzinger, J., and Milliken, R., Ed., Sedimentary geology of Mars, SEPM.Society for Sedimentary Geology Special Publication 102, p. 97-117.

Wang, Alian, Bell, J. F., Li, Ron, Johnson, J. R., Farrand, W. H., Cloutis, E. A., Arvidson, R. E., Crumpler, L., Squyres, S. W., McLennan, S. M., Herkenhoff, K. E., Ruff, S. W., Knudson, A. T., Chen, Wei, and Greenberger, R. (2008) Light-toned salty soils and coexisting Si-rich species discovered by the Mars Exploration Rover Spirit in Columbia Hills. Journal of Geophysical Research, 113, E12S40. doi.org/10.1029/2008JE003126.

Wray, J. J., Murchie, S. L., Squyres, S. W., Seelos, F. P., and Tornabene, L. L. (2009) Diverse aqueous environments on ancient Mars revealed in the southern highlands. Geology, 37, 1043–1046. doi: 10.1130/G30331A.1.

Yen, Albert S., Gellert, Ralf, Schröder, Christian, Morris, Richard V., Bell, James F., Knudson, Amy T., Clark, Benton C., Ming, Douglas W., Crisp, Joy A., Arvidson, Raymond E., Blaney, Diana, Brückner, Johannes, Christensen, Philip R., Desmarais, David J., de Souza, Paulo A., Economou, Thanasis E., Ghosh, Amitabha, Hahn, Brian C., Herkenhoff, Kenneth E., Haskin, Larry A., Hurowitz, Joel A., Joliff, Bradley L., Johnson, Jeffrey R., Klingelhöfer, Göstar, Madsen, Morten Bo, McLennan, Scott M., McSween, Harry Y., Richter, Lutz, Rieder, Rudi, Rodionov, Daniel, Soderblom, Larry, Squyres, Steven W., Tosca, Nicholas J., Wang, Alian, Wyatt, Michael and Zipfel, Jutta. (2005) An integrated view of the chemistry and mineralogy of martian soils. Nature, 436, 49-54.

Yen, A. S., Morris, R. V., Clark, B. C., Gellert, R., Knudson, A. T., Squyres, S., Mittlefehldt, D. W., Ming, D. W., Arvidson, R., McCoy, T., Schmidt, M., Hurowitz, J., Li, R., and Johnson, J.

R. (2008). Hydrothermal processes at Gusev crater: An evaluation of Paso Robles class soils. Journal of Geophysical Research,113, E06S10.

Table 1. Derived Compositions of Vein and Coating

Element	Esperance 6 (RAT grind)	Esperance2 (as-is)	Derived Compositions Vein	Derived Compositions Coating
Na2O	2.25	2.16	2.28	1.98
MgO	4.73	6.49	4.19	10.15
Al2O3	15.37	10.36	16.90	0.00
SiO2	62.45	50.56	66.08	25.77
P2O5	1.14	1.26	1.11	1.49
SO3	3.28	8.93	1.55	20.70
Cl	2.32	2.61	2.23	3.21
K2O	0.24	0.45	0.18	0.89
CaO	2.14	5.80	1.02	13.42
TiO2	0.93	0.99	0.92	1.12
Cr2O3	0.34	0.28	0.35	0.17
MnO	0.19	0.27	0.16	0.44
FeO	4.43	9.59	2.86	20.34
Ni (ppm)	622	707	596	884
Zn (ppm)	238	484	163	995
Br (ppm)	35	233	0	644

Table 2. Additional Measured Compositions

Element	Lihir As-Is	Esp1 As-Is	Esp3 As-Is (sum)	Esp4 As-Is	Esp5 (RAT grind)	Typical Soil (ave.)
Na2O	1.66	2.28	2.25	2.28	2.54	2.34
MgO	5.89	6.19	6.13	6.12	4.79	7.33
Al2O3	12.92	11.47	11.36	11.72	14.61	9.65
SiO2	58.44	53.29	53.89	55.47	61.04	46.97
P2O5	1.19	1.30	1.23	1.15	1.19	0.85
SO3	6.25	7.88	7.88	7.28	3.98	4.68
Cl	1.58	2.53	2.95	2.97	2.80	0.59
K2O	0.37	0.39	0.42	0.39	0.25	0.51
CaO	4.03	5.05	4.56	3.93	2.49	7.38
TiO2	1.16	1.02	1.01	1.04	0.95	0.90
Cr2O3	0.32	0.30	0.30	0.28	0.34	0.39
MnO	0.16	0.28	0.23	0.23	0.19	0.39
FeO	5.80	7.81	7.55	6.93	4.64	17.57
Ni (ppm)	644	606	670	728	633	349
Zn (ppm)	304	377	413	361	253	199
Br (ppm)	114	213	142	144	58	24
Sum	99.78	99.80	99.77	99.78	99.81	99.55

Table 3. Classification characteristics for comparing high-Si samples analyzed by the Spirit and Opportunity rovers.

Criterion	Kenosha _Comets	Fuzzy _Smith	Independance _Penn2	Esperance6
Cr/Fe	V. High	low	low	High
Cr/Si	typical	v. low	v. low*	typical
Ti/Si	typical	High**	High*	typical
K2O (wt%)	0.2	2.8	0.5	0
Ti/Fe	V. High	High	High*	typical
Al/Si	v. low	v. low	V. High	V. High
FeO (wt%)	1.07	6.76	3.85	4.43
	*Ti is unusually high, Cr low in Wishstone/Watchtower/Independence			
	**~75% higher than Kenosha or Esperance			

FIGURE CAPTIONS

Fig. 1. Esperance and Lihir analysis locations are part of the boxwork seen in this Pancam enhanced-color image.

Fig. 2. Merge of MI and Pancam L257 color images of the Esperance fracture filling vein material (whitish) with dark coatings (patchy areas to right). A lag gravel borders the brighter slope, to the left. Area shown ~5 x 5 cm; illumination from left. (Sol 3267, image ID 1MPW67IOFBYORT00P2955L257F1). Arrow points to a newberry.

Fig. 3(a). Anaglyph (red/blue) of Esperance, generated from MI focal sections acquired on Sol 3267, before RAT grinding. Field of view is 3x3 cm square, illumination from right (note: this series of images is rotated 180 degrees relative to those shown in other figures to facilitate stereo viewing).

Fig. 3(b). (left) Part of MI orthomosaic of focal merges of images acquired on Sol 3298 of target Esperance4. (right) Topographic profile along the red arrow, demonstrates the stepped, coated plateaus and the steep drop-off of the bright material at lower right. Elevation in mm.

Fig. 3(c). Oblique microtopographic representations of the DEM of Fig. 3(b), clearly showing the prevalence of surviving coating on higher, flat areas. (top) MI orthophoto draped over DEM. (bottom) Rainbow color-coded topography (red=high, purple=low) on shaded relief.

This is a preprint, the final version is subject to change, of the American Mineralogist (MSA)
Cite as Authors (Year) Title. American Mineralogist, in press.
(DOI will not work until issue is live.) DOI: http://dx.doi.org/10.2138/am-2016-5575

Fig. 4. Lihir target. (top) MI image 1M415738717EFFBXN2P2905M2M1, 3x3 cm across,with illumination from right, showing APXS placement (white circle). Area shown about 2x2 cm across.

Fig. 5(a). Pancam image taken after grinding of Esperance with the RAT on sol 3305. Powdered material is gray, rather than the reddish coloration for grindings of Burns Formation and other ferric-rich chemical sediments on Mars.

Fig. 5(b). Mosaics of MI images of Esperance5 acquired on Sol 3301 with illumination from upper left. (top) RAT grinding removed most, but not all of the dark coating material (e.g., the segment within the yellow dashed triangle). Three embedded spherules that have been partially ground are denoted by blue arrows. Three additional roundish features are marked by white arrows. Area shown about 4 cm across. (bottom) Merge of MI mosaic with Pancam L257 enhanced color. Area shown about 5x5 cm across.

Fig. 6. Spectral features taken with Pancam filters for Esperance coating and bright vein material.

Fig. 7. Grinding to produce Esperance6 composition from Esperance4 and Esperance5 causes Al and Si to increase strongly, and elements such as S, Fe, Ca and Mg to decrease significantly, demonstrating that the vein material is composed primarily of Si and Al.

Fig. 8. Trends are well defined for most major and minor elements. (top) Particularly noteworthy is the positive correlation of Al_2O_3 (e.g., aluminosilicate) and the general extrapolation by other elements to a SiO_2-rich end-member. (bottom) Al_2O_3 is strongly

anti-correlated with SO_3, while CaO is strongly correlated positively, with extrapolation through (0,0). In contrast, Mg also has a clear trend with SO_3, but the extrapolated trend line clearly shows that a significant fraction of Mg is also associated with some other phase.

Fig. 9. Al_2O_3 does not extrapolate to (0,0), indicating the presence of additional SiO_2 in the system which is not in the form of an aluminosilicate.

Fig. 10. The Cr variation with SiO_2 does intersect at (0,0), with a correlation R^2 of ~ 0.8 and slope indicating 0.48% of the value of SiO_2, in both the vein and its coating. No correlation with TiO_2 is evident.

Fig. 11. Selected correlation coefficients (R-values) across all eight measurements for the strong correlations with cardinal elements Si, Fe and S (from 120 element pairs). Dashed lines highlight the strongest positive correlations.

Fig. 12. Although Br is typically highly variable and erratic for most in situ sample analyses on Mars, and Zn commonly shows major fluctuations, both trace elements are well correlated with SO_3 content in the Esperance coating, whereas trace element Ni is not.

Fig. 13. Abundances of S and Cl for various Esperance samples, and martian soils. Highest S abundances occur for cases with the greatest areal coverage of the

discontinuous coating material. Note the higher Cl abundances than soils, and the approximate constancy of Cl independent of changes in S as grinding operations remove coating material (left to right).

Fig. 14. Composition of Vein Material

Fig. 15. Composition of Coating

Fig. 16. Comparison of compositions with terrestrial montmorillonites from field occurrences. Concentrations of the elements shown have been normalized to total 100 wt% on a H_2O and OH-free basis. Esperance vein material is somewhat high in SiO_2, indicating the possible presence of a Si-rich accessory mineral, such as some form of silica (see text for discussion). Esperance* is the aluminosilicate composition if one-sixth of the SiO_2 is allocated to silica.

769 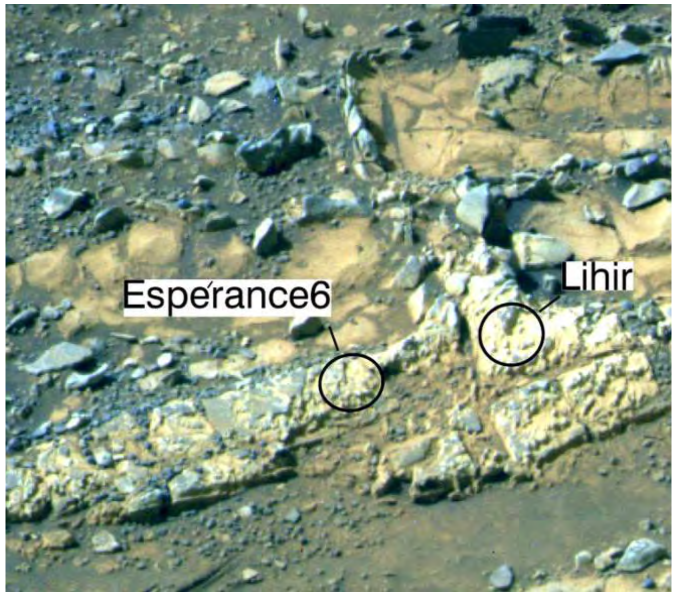

770 Fig. 1.

771

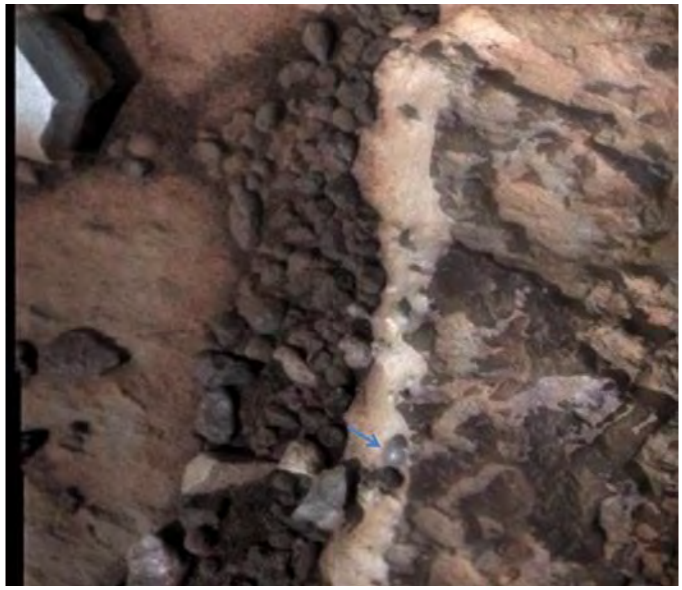

Fig. 2.

776 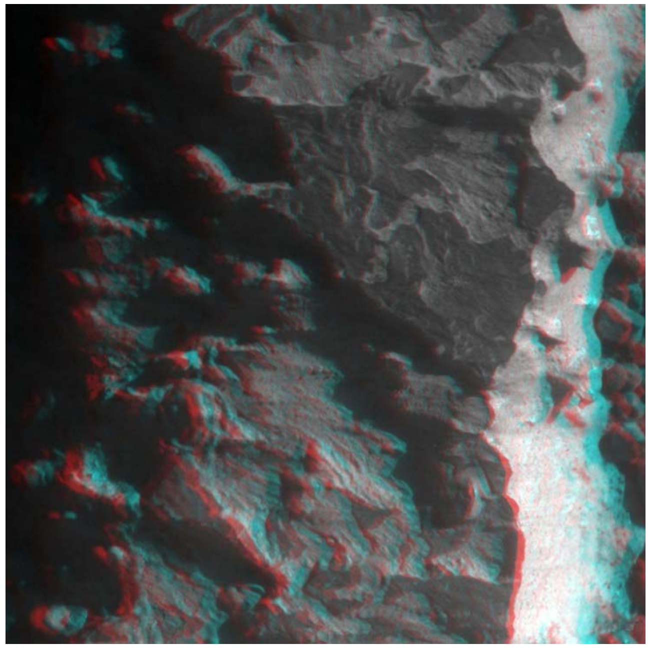

777 Fig. 3(a).

778

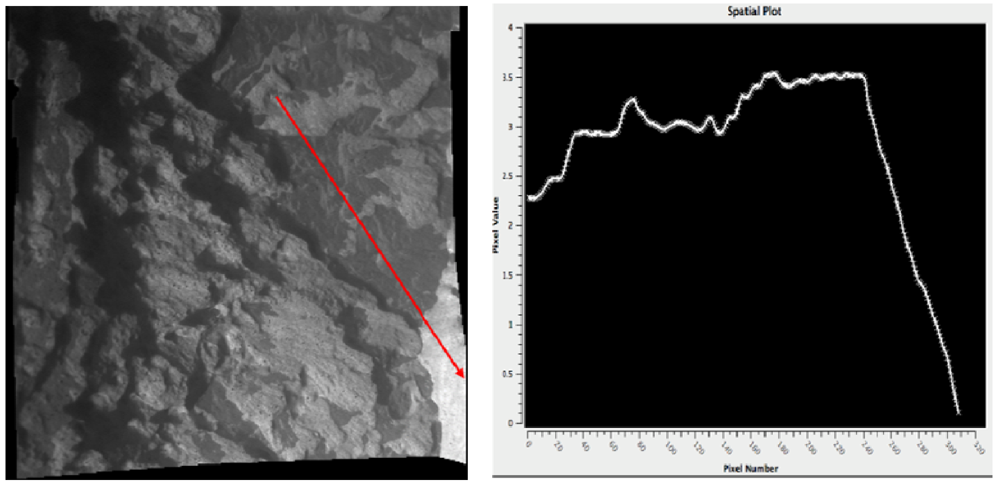

Fig. 3(b).

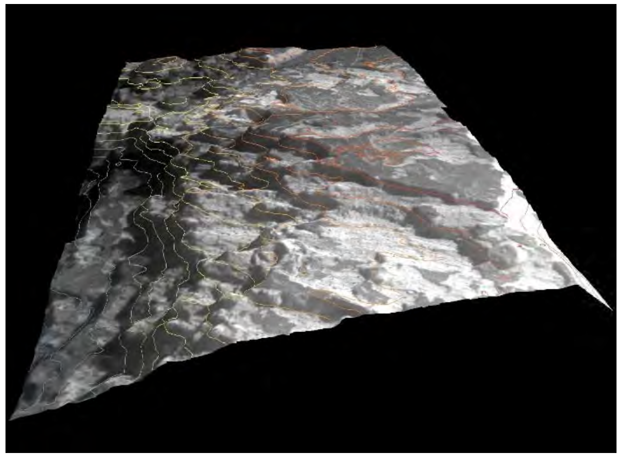

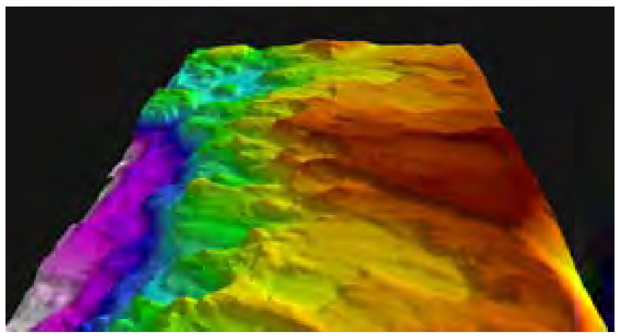

Fig. 3(c).

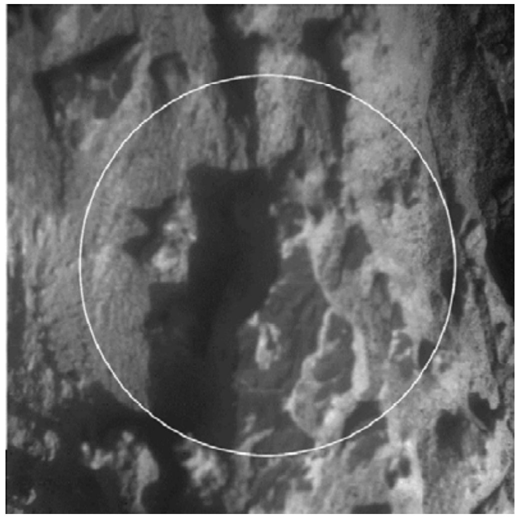

Fig. 4.

This is a preprint, the final version is subject to change, of the American Mineralogist (MSA)
Cite as Authors (Year) Title. American Mineralogist, in press.
(DOI will not work until issue is live.) DOI: http://dx.doi.org/10.2138/am-2016-5575

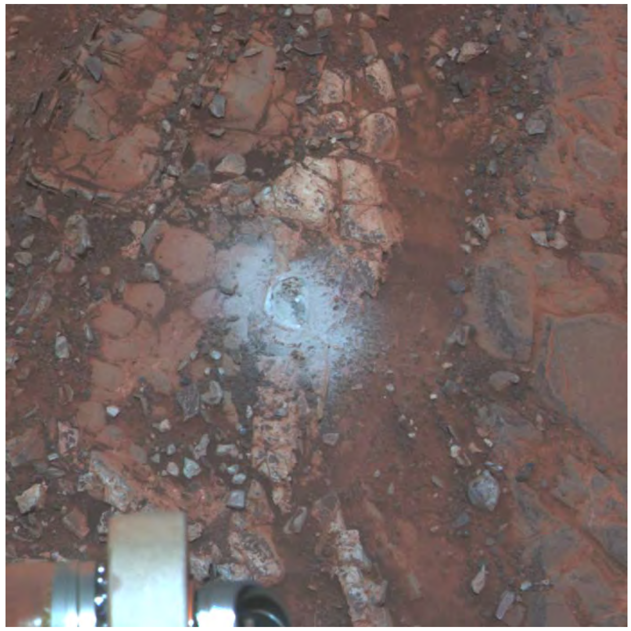

Fig. 5(a).

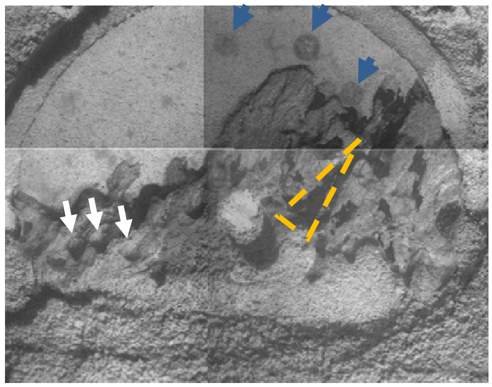

Fig. 5(b).

This is a preprint, the final version is subject to change, of the American Mineralogist (MSA)
Cite as Authors (Year) Title. American Mineralogist, in press.
(DOI will not work until issue is live.) DOI: http://dx.doi.org/10.2138/am-2016-5575

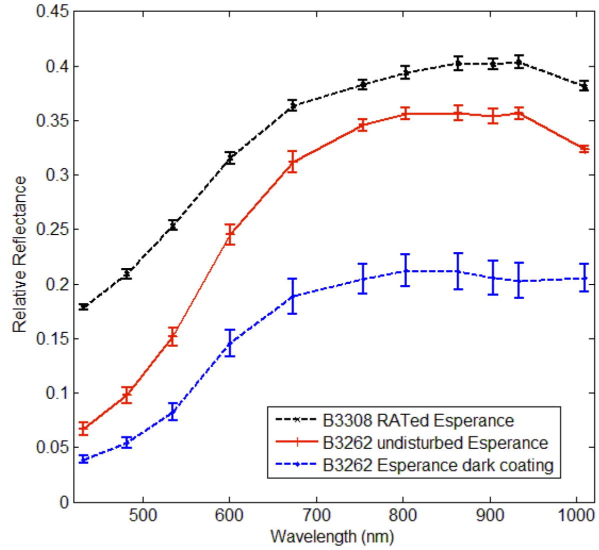

800

801 Fig. 6.

802

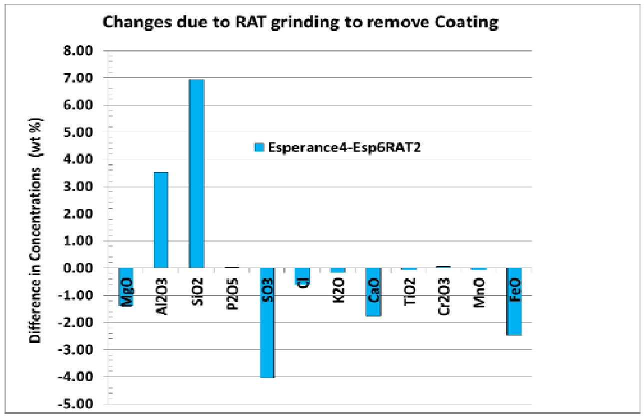
Changes due to RAT grinding to remove Coating
Difference in Concentrations (wt %)
8.00
7.00
6.00
5.00
4.00
3.00
2.00
1.00
0.00
-1.00
-2.00
-3.00
-4.00
-5.00
Esperance4-Esp6RAT2
MgO
Al2O3
SiO2
P2O5
SO3
Cl
K2O
CaO
TiO2
Cr2O3
MnO
FeO

Fig. 7.

This is a preprint, the final version is subject to change, of the American Mineralogist (MSA)
Cite as Authors (Year) Title. American Mineralogist, in press.
(DOI will not work until issue is live.) DOI: http://dx.doi.org/10.2138/am-2016-5575

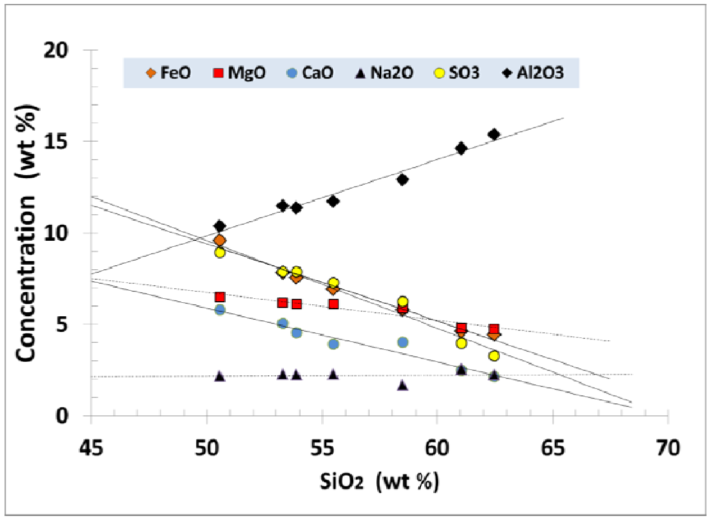

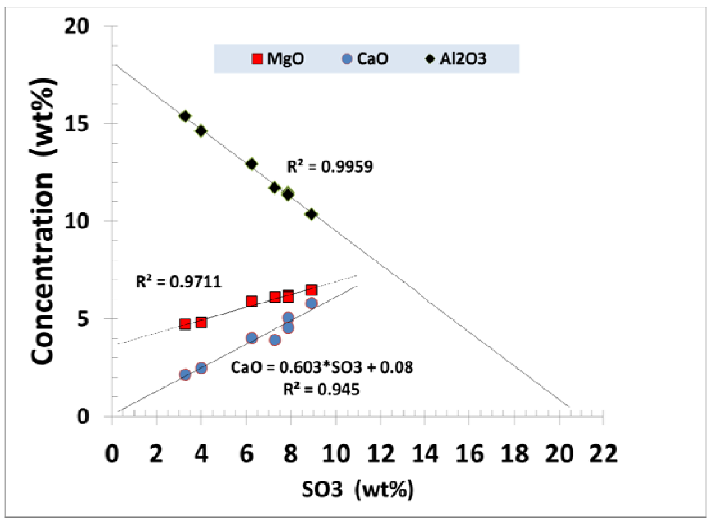

Fig. 8.

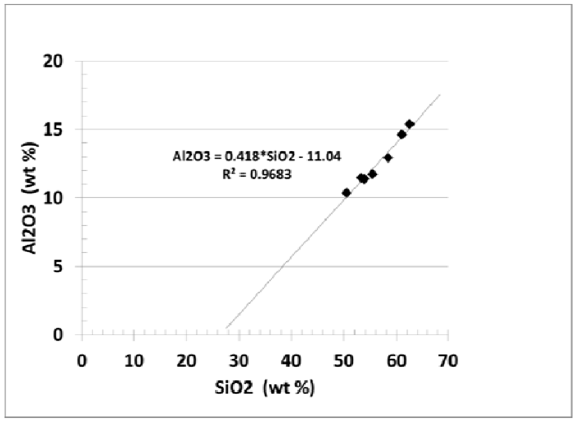
Al2O3 = 0.418*SiO2 - 11.04
R² = 0.9683
Al2O3 (wt %)
SiO2 (wt %)
0
5
10
15
20
0
10
20
30
40
50
60
70

Fig. 9.

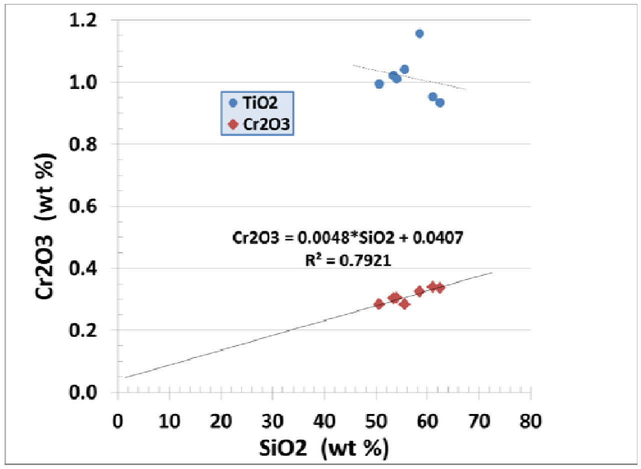
TiO2
Cr2O3
Cr2O3 = 0.0048*SiO2 + 0.0407
R² = 0.7921
Cr2O3 (wt %)
SiO2 (wt %)
0.0
0.2
0.4
0.6
0.8
1.0
1.2
0
10
20
30
40
50
60
70
80

Fig. 10.

	SiO2
SiO2	1
Al2O3	0.9795
Cr2O3	0.9419
TiO2	-0.066
Na2O	-0.208
Cl	-0.255
Ni	-0.262
P2O5	-0.627
MnO	-0.877
K2O	-0.927
Zn	-0.948
MgO	-0.957
Br	-0.96
CaO	-0.971
SO3	-0.974
FeO	-0.992

	FeO
FeO	1
CaO	0.965
SO3	0.9524
Br	0.9517
MgO	0.9457
Zn	0.9419
K2O	0.9146
MnO	0.8682
P2O5	0.5885
Ni	0.2464
Cl	0.2207
Na2O	0.2007
TiO2	0.0405
Al2O3	-0.959
Cr2O3	-0.962
SiO2	-0.992

	SO3
SO3	1
MgO	0.9917
K2O	0.9765
CaO	0.9681
FeO	0.9524
Zn	0.9521
Br	0.9404
MnO	0.7867
P2O5	0.5655
Ni	0.3602
TiO2	0.2309
Cl	0.1713
Na2O	0.025
Cr2O3	-0.895
SiO2	-0.974
Al2O3	-0.999

Fig. 11.

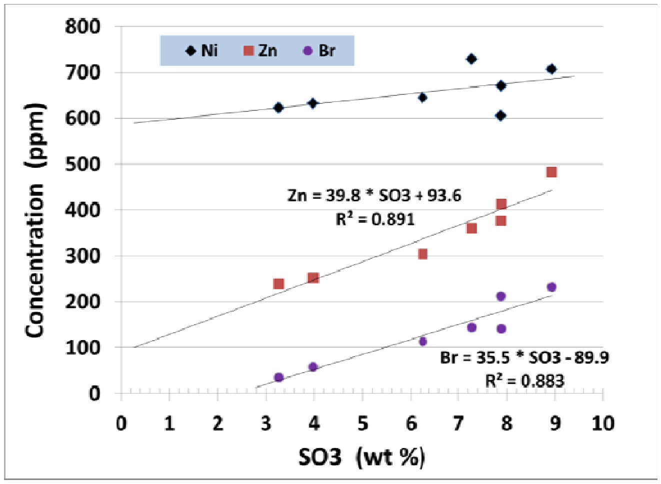
Ni
Zn
Br
Zn = 39.8 * SO3 + 93.6
R² = 0.891
Br = 35.5 * SO3 - 89.9
R² = 0.883
Concentration (ppm)
SO3 (wt %)
0
100
200
300
400
500
600
700
800
0 1 2 3 4 5 6 7 8 9 10

Fig. 12.

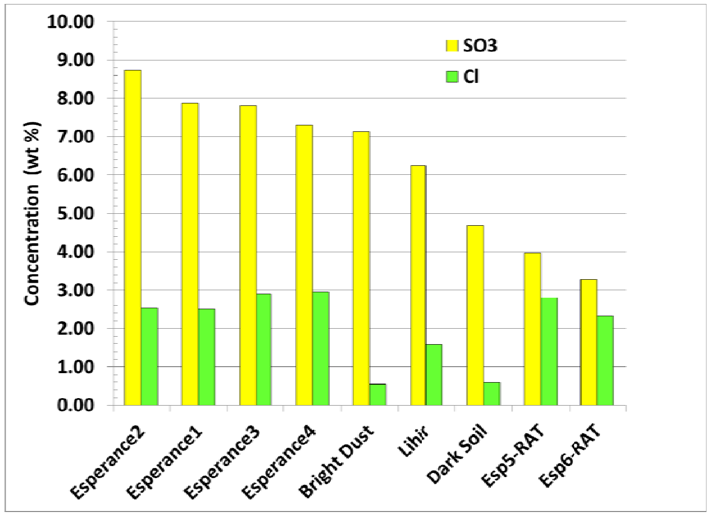
Concentration (wt %)
10.00
9.00
8.00
7.00
6.00
5.00
4.00
3.00
2.00
1.00
0.00
SO3
Cl
Esperance2
Esperance1
Esperance3
Esperance4
Bright Dust
Lihir
Dark Soil
Esp5-RAT
Esp6-RAT

Fig. 13.

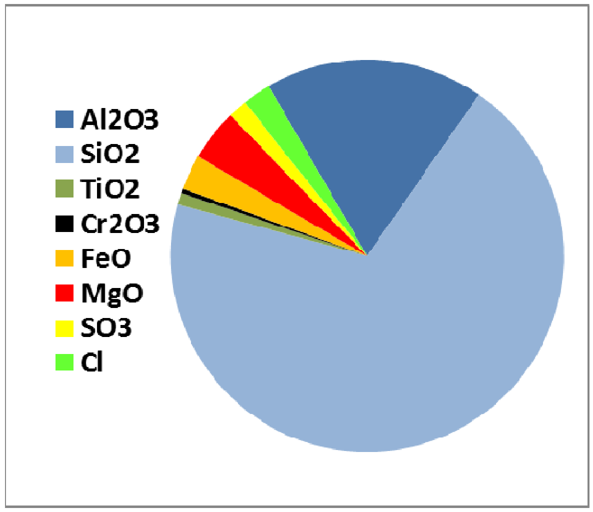

Fig. 14.

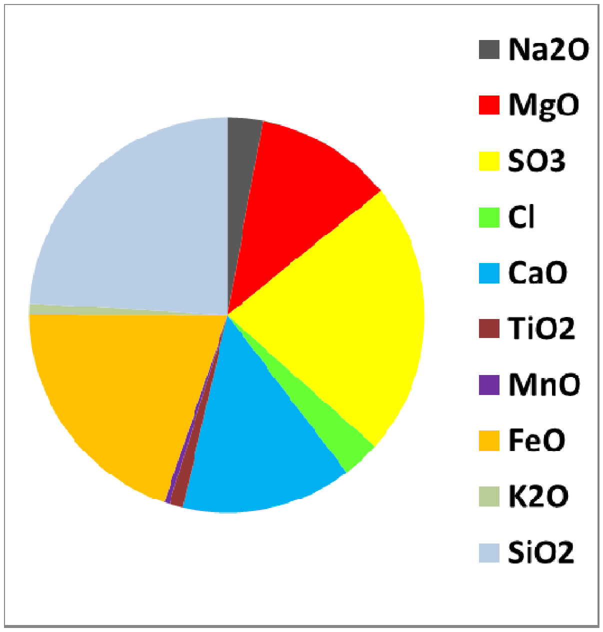

Fig. 15.

This is a preprint, the final version is subject to change, of the American Mineralogist (MSA)
Cite as Authors (Year) Title. American Mineralogist, in press.
(DOI will not work until issue is live.) DOI: http://dx.doi.org/10.2138/am-2016-5575

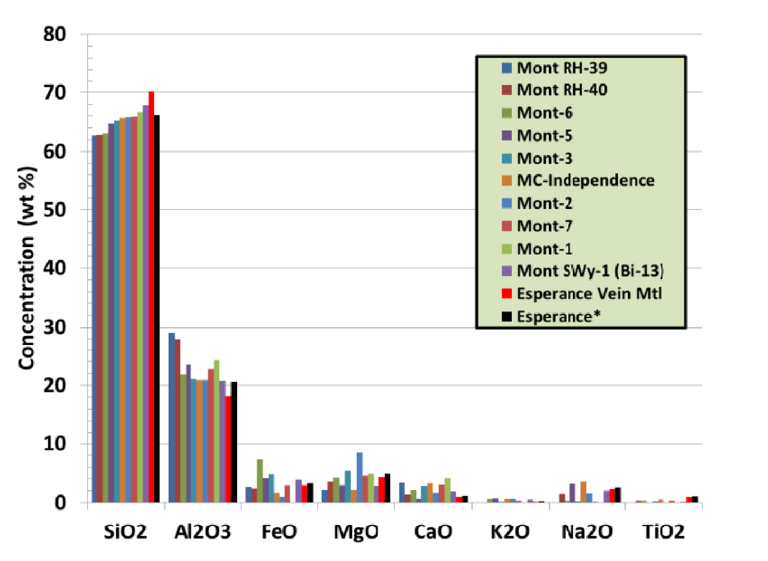

Fig. 16.